Bulletin of the Seismological Society of America. Vol. 68, No. 1, pp. 31–48. February 1978

PREDICTABILITY OF STRONG GROUND MOTION IN THE IMPERIAL VALLEY: MODELING THE M4.9, NOVEMBER 4, 1976 BRAWLEY EARTHQUAKE

By Thomas H. Heaton and Donald V. Helmberger

ABSTRACT

Strong-motion displacements, recorded at 33 km (IVC) and 36 km (ELC) from the November 4, 1976 Brawley earthquake, are modeled using the Cagniard-deHoop technique. The IVC record consists almost entirely of transversely polarized motion, whereas the ELC record contains an approximately equal proportion of transversely and radially polarized motion. A simplified shear-wave velocity model was determined from the compressional wave refraction studies of Biehler, Kovach, and Allen (1964). The epicentral location and focal mechanism computed from *P*-wave first-arrival studies were used to locate and orient a double-couple point source within the layered half-space. The far-field time function and source depth were the only parameters without good independent constraints. A triangular far-field time function with a duration of 1.5 sec and a source depth of 7 km were sufficient to model the first 25 sec of tangential ground motion. It appears that the effects of velocity structure on the propagation of long-period *SH* waves are predictable in the Imperial Valley. A study of the synthetic Fourier amplitude spectra indicates that wave propagation effects should be included in studies of source spectra and seismic wave attenuation.

Introduction

The Imperial Valley of Southern California is unusual in that it has the rare combination of flat lying sediments and earthquakes. Furthermore, the upper crustal velocity structure has been studied extensively by Biehler (1964). The Imperial Valley is thus particularly well suited for wave-form modeling studies of strong ground motion from local earthquakes. In this paper, we will examine the tangentially polarized ground motion from a M_L 4.9 earthquake which occurred on November 4, 1976. Our approach will be to use a velocity structure model which is based on Biehler's work, along with the calculated hypocentral location and fault-plane solution, to predict the tangentially polarized ground motion observed for this earthquake. Previous modeling of local *SH* wave forms (Helmberger and Malone, 1975; Heaton and Helmberger, 1977) has been somewhat unsatisfying because velocity structure as well as source model parameters have been constrained primarily by the condition that synthetic and observed wave forms match each other. Obviously, any successful model must satisfy this constraint, but due to questions of uniqueness and the applicability of plane layered structure models to complexly faulted regions, one cannot help but feel that the choice of model parameters seemed somewhat *ad hoc*. In view of this objection, we pose the following question: Is it possible to predict the motion from an earthquake using a model whose velocity structure parameters are determined independently of the wave-form modeling? We will show that the answer in this particular case is yes! Thus we will demonstrate a model which is consistent with both the observed wave forms and the independent constraints on velocity structure and epicentral location.

We will also investigate the effect of changes in the model parameters on the syn-

thetic wave forms. Since we used generalized ray theory to generate the synthetics, it is possible to associate arrivals on the record with specific travel paths. Although we prefer to view our models in the time domain, we will also present Fourier amplitude spectra of our synthetics. We will show that synthetic amplitude spectra for layered half-spaces are significantly different than spectra calculated for a homogeneous half-space. The effects of structure must be included when making estimates of source parameters or seismic wave attenuation.

The November 4 Brawley Earthquake

During the period from November 3 through November 8, 1976, a swarm of more than 400 earthquakes was recorded by the U.S. Geological Survey Imperial Valley short-period seismic array. This swarm occurred approximately 15 km northwest of a well-studied swarm which occurred along the Brawley fault in February of 1975 (Johnson and Hadley, 1976). Unlike the February 1975 swarm, which produced significant surface deformation (Sharp, 1976), no surface deformation has yet been associated with the November 1976 swarm. The largest event in the November 1976 swarm occurred at 10:41 GMT on November 4 and was assigned a magnitude of 4.9. By using P-wave arrival times from the Imperial Valley seismic array, the epicentral location (shown in Figure 1) was determined by the U.S. Geological Survey to be 33°05′ North latitude and 115°36′ West longitude (Madeline Schnapp and Gary Fuis, personal communication). The USGS hypocentral depth was $4\frac{1}{2}$ km with low P residuals. However, we prefer a depth of 7 km based on our modeling of strong-motion wave forms. Since the hypocenter is only loosely constrained by P for these solutions, this difference does not appear significant. Assuming a hypocentral depth of 7 km, we computed a focal mechanism using P-wave first-motion data from 68 stations in the joint Caltech-USGS Southern California seismic array. The focal mechanism, which is shown in Figure 2, indicates predominantly right-lateral faulting along a steeply dipping fault which trends N-NW. Because the motion is mostly strike-slip along a vertical plane, this solution is relatively insensitive to changes in the assumed hypocentral depth.

Two long-period strong-motion seismic stations were triggered during the swarm sequence. A three-component 4X torsion seismometer with a free period of 10 sec was located at Imperial Valley College (IVC) at a distance of 33 km from the epicenter (see Figure 1). This instrument records on photographic paper on a revolving drum for a full 24 hours after being triggered. The instrument triggered 6 hours before the M4.9 earthquake being studied in this paper and thus the entire wave train of the earthquake was well recorded. Shown in Figure 3 are the records from IVC. The instrument response has been deconvolved and the resulting ground motion has been heavily filtered at periods longer than 20 sec with an Ormsby filter (Hudson *et al.*, 1971). Unfortunately, the vertical torsion recording shows a long-period drift near the onset of motion which seems to have a positive net area. This indicates some nonlinearity in the instrument response which made deconvolution impossible. Despite this, it seems clear from the original records that horizontal ground motion was much larger than vertical ground motion. Also shown in Figure 3 are the displacements rotated into radial and tangential directions. An inspection of these rotated motions clearly shows that the ground motion at IVC was dominated by transversely polarized shear waves, as would be expected, since IVC lies near a P-SV node (Figure 2).

A second recording of ground motion was made by the horizontal Carder displacement meters located in El Centro at a distance of 36 km. No long-period vertical in-

strument is present at this station. The horizontal instruments have a static magnification of 1.0 with free periods near 6 sec. These instruments appear to have triggered

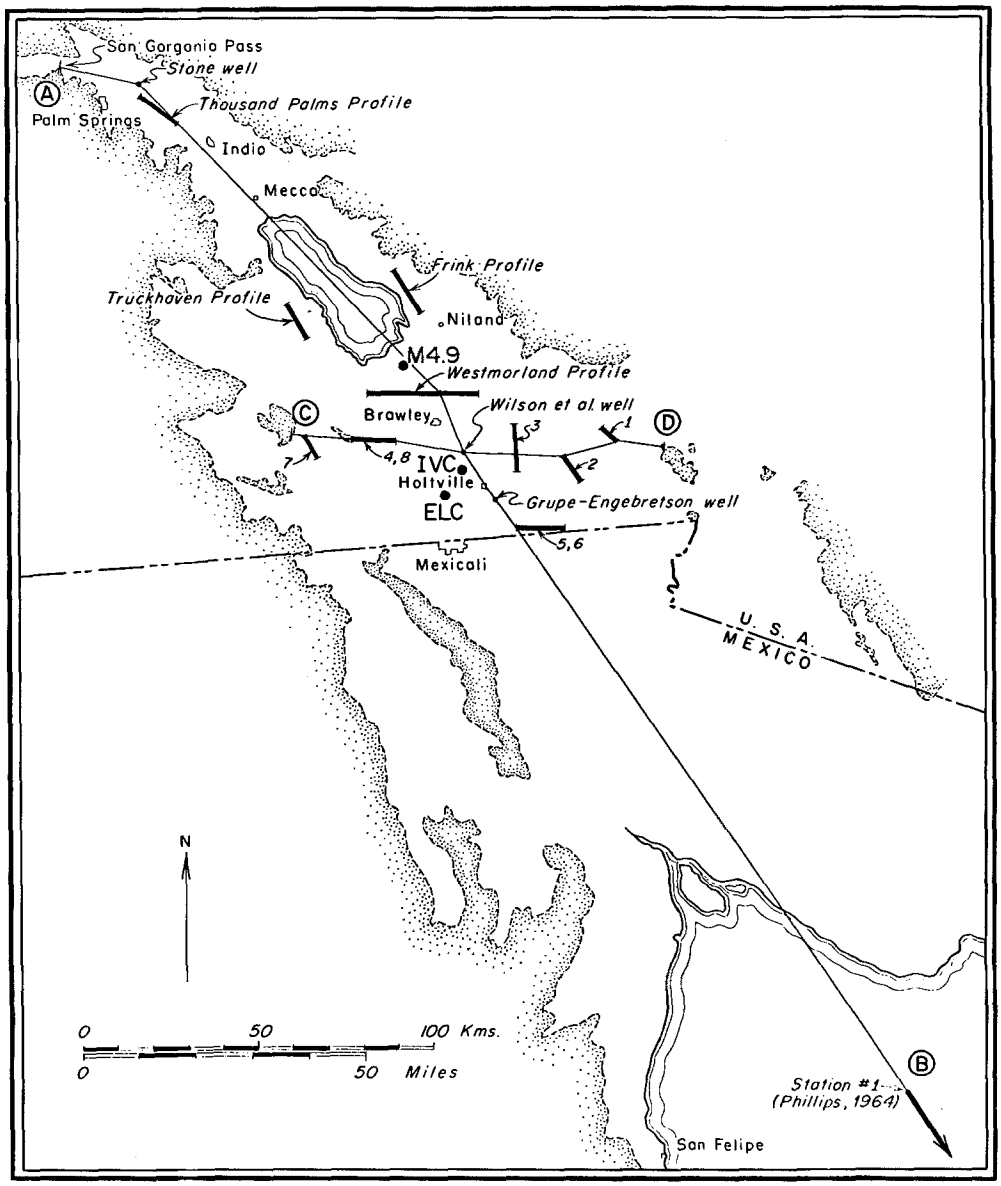

FIG. 1. Index map of Salton trough showing locations of seismic refraction profiles and cross-section lines A—B (Fig. 5a) and C—D (Fig. 5b). Also shown are the long-period strong-motion stations, IVC and ELC, and the epicenter of the $M4.9$, November 4, 1976 earthquake. Stippling indicates generalized outline of pre-Tertiary crystalline rocks bordering the Salton trough. This figure has been modified from Biehler, Kovach, and Allen (1964).

near the start of the S wave and thus the beginning of the record is lost. The records from ELC are shown in Figure 4. Also shown is the ground motion obtained by deconvolution of the instrument response and Ormsby filtering of periods beyond 15 sec. Since the beginning of the record was lost, the deconvolution of the first pulse on the record is questionable. Rotation of the displacements indicates that there

were much larger radial displacements at ELC than there were at IVC. The fact that the radial and tangential wave forms are quite dissimilar suggests that this change in

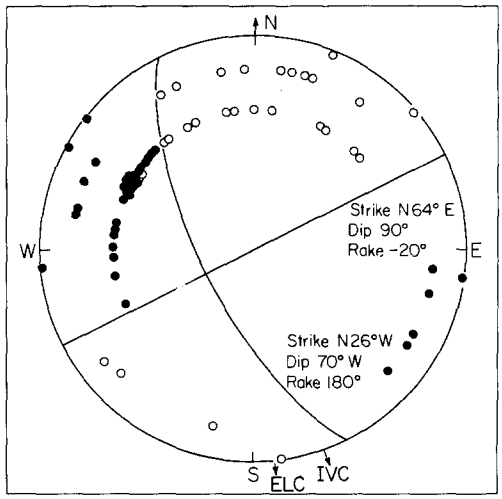

FIG. 2. Focal mechanism for the $M4.9$, November 4 earthquake determined from P-wave first motions observed at 68 stations in the joint Caltech-USGS Southern California seismic array. The azimuths of the stations, IVC and ELC, are also shown.

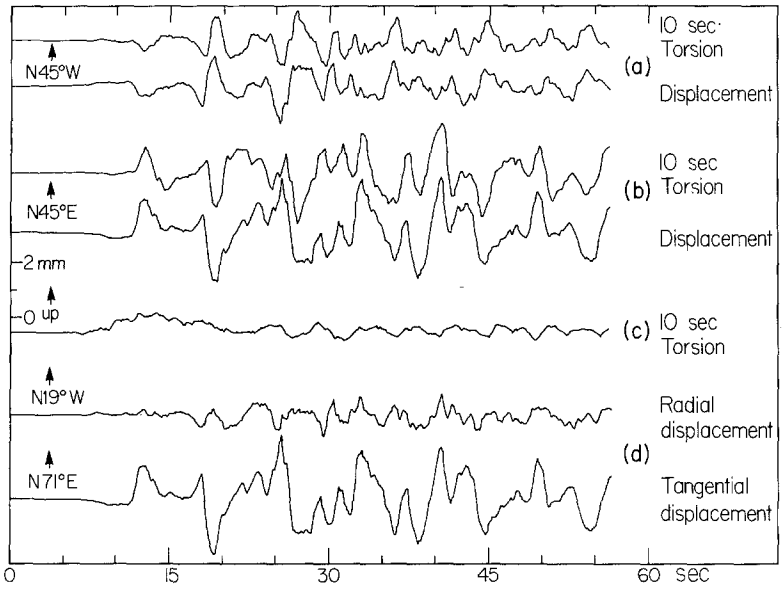

FIG. 3. Summary of ground motion observed at IVC. (a) NW component of ground motion with and without the instrument response. (b) NE component of ground motion with and without instrument response. (c) Vertical component of ground motion with the instrument response. The instrument response could not be deconvolved because of the long-period arrival which appears to have a net positive area. (d) Ground motion rotated into radial and tangential components.

amplitude ratios is not due to a poor rotation of predominantly transverse motions. The difference in the magnitude of radial displacements between ELC and IVC is consistent with the fact that the azimuth of ELC is further from the P and SV node shown in Figure 2. Notice that there is a remarkable degree of coherence between the

tangential wave forms recorded at IVC and ELC. This is as it should be since the differences in range and azimuth between ELC and IVC are only 3 km and 13°, respectively.

Crustal Structure in the Salton Trough

The Salton trough is a structural depression which is the northward continuation of the Gulf of California. This depression is underlain and bounded by Mesozoic and older crystalline rocks. As much as 6 km of upper Tertiary and Quaternary marine and nonmarine sediments fill this depression. Also present in the Salton trough are several major active right-lateral fault zones, recent volcanism, and potential geo-

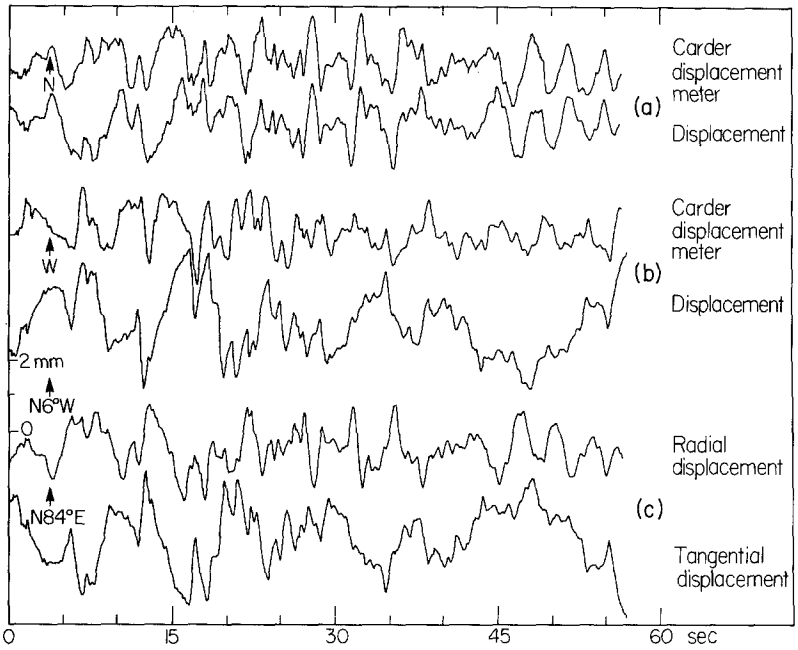

Fig. 4. Summary of ground motion observed at ELC. Since this instrument was probably triggered by the direct *S* wave, the beginning of the record is lost. (a) North component of ground motion with and without instrument response. (b) West component of ground motion with and without instrument response. (c) Ground motion rotated into radial and tangential components. No long-period vertical strong-motion instrument is present at this station.

thermal reserves. The November 1976 Brawley swarm as well as the stations, IVC and ELC, lie near the axis of this depression. The work of Biehler *et al.* (1964) on *P*-wave refraction profiles indicates that there is very little variation in upper crustal velocity structure along the axis of the Salton trough. This is illustrated by the cross section A—B which is shown in Figure 5a. Although the total thickness of sediments varies considerably as one travels perpendicular to the axis of the trough, the depths of individual layers within the sediments are amazingly consistent as one crosses the Salton trough. This can be seen in the cross section C—D shown in Figure 5b. Thus the overall impression of sedimentary structures down the axis of the trough is one of relatively plane layers.

Unfortunately, there are several reasons why the velocity models calculated by Biehler *et al.* (1964) cannot be used directly in our modeling. Most importantly, we need to know shear-wave velocities and the refraction studies were for only com-

pressional waves. Also, a model which consists of five layers over a half-space requires the computation of too many generalized rays to be practical. Shawn Biehler (personal communication) has indicated that the interfaces above and below the layer with a compressional wave velocity of 2.6 km/sec were the sharpest and most consistently

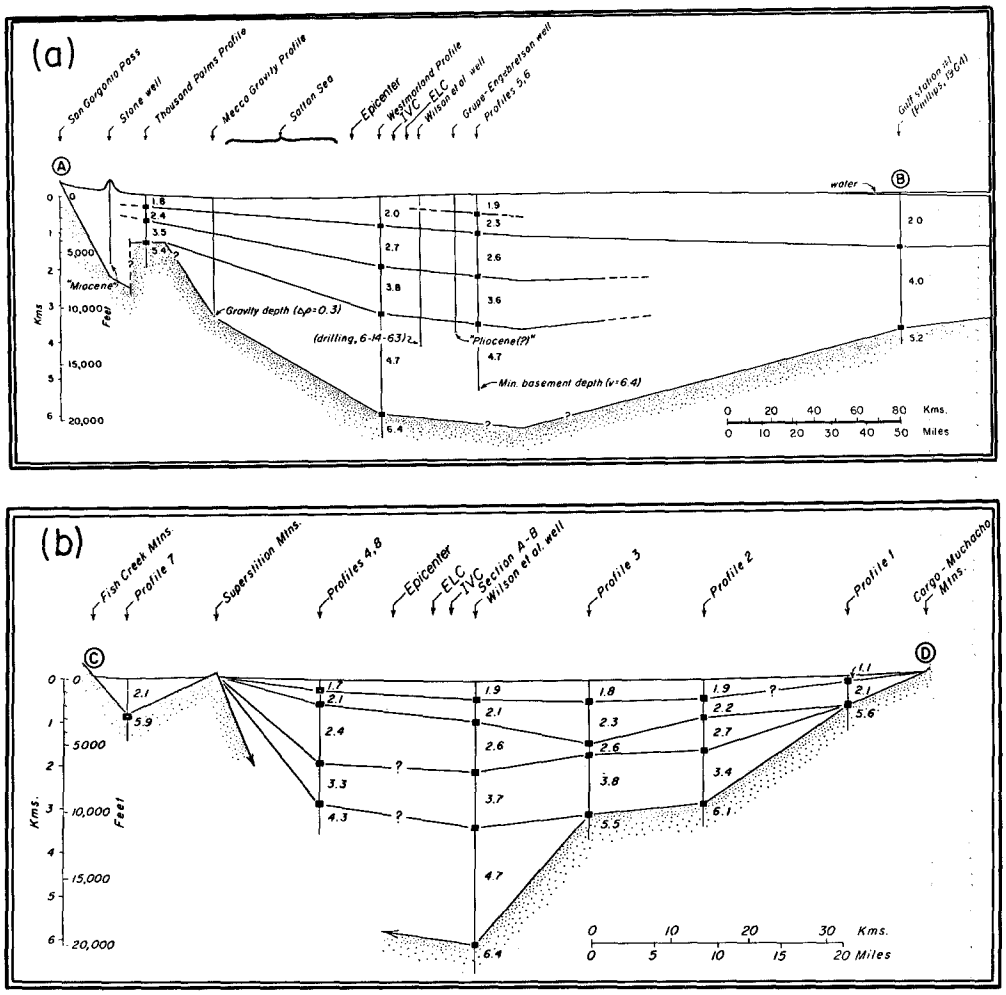

FIG. 5. (a) Seismic cross section along line A—B of Figure 1. Numbers indicate velocities in km/sec. (b) Seismic cross section along line C—D of Figure 1. Note that the ratio of horizontal-to-vertical scales is different on part (a) than on part (b). Also notice that the structure is relatively flat along the paths from the epicenter to the stations, IVC and ELC. These figures have been modified from Biehler *et al.* (1964).

observed interfaces found in the region. He also believes that the sediment-to-basement velocity contrast is very sharp. We thus condensed the five-layered model into one with three layers by combining layers one and two and also layers four and five. This is shown in Table 1. In order to convert these compressional wave velocities to shear-wave velocities, we chose a Poisson ratio of 0.25 for everything except the uppermost layer. A Poisson ratio of 0.35 was assumed for the uppermost kilometer of very soft sediments as suggested by Ronald Scott (personal communication). The S-wave model given in Table 1 is the one which was used throughout this study.

Description of the Modeling Technique

Our basic modeling tool will be the Green's function, J_j (t), which represents the response of a layered elastic half-space to a point shear dislocation. The response is calculated by using the generalized ray method. The solution is represented by the sum of the responses of individual generalized rays, each of which traverses a different path which is characterized by the interfaces it contacts. The response of each generalized ray was computed by using the Cagniard-de Hoop technique. The complete solution containing both near-field and far-field terms for dislocation sources embedded in a layered half-space has been discussed by Helmberger (1974) and Vered and Ben-Menahem (1974). For the periods and station ranges of interest in this study, it is sufficient to model only the far-field term so that the asymptotic solution can be used (see Helmberger and Malone, 1975). These approximations become progressively better for shorter periods. We have found it convenient to view our responses in terms of the displacement, $J_j(t)$, due to a dislocation time history which consists of a ramp function (far-field step function response). The surface tangential

TABLE 1

Thickness (km)	P Velocity (km/sec)	Thickness (km)	P Velocity (km/sec)	S Velocity (km/sec)	Density (g/cc)
0.45	1.7	0.95	2.0	0.88	1.8
0.5	2.1				
1.15	2.6	1.15	2.6	1.5	2.35
1.3	3.7	3.8	4.2	2.4	2.6
2.5	4.7				
	6.4		6.4	3.7	2.8

component of motion produced by an arbitrarily oriented point dislocation as described by Langston and Helmberger (1975) is given by

$$V(r, \theta, 0, t) = \frac{M_0}{4\pi\rho_0} F(t) * \frac{d}{dt} \sum_{j=1}^{2} A_{j+3} J_j(t), \tag{1}$$

where M_0 is fault moment, ρ_0 is density at the source, $F(t)$ is the far-field time history, $(dS(t)/dt)$, and $S(t)$ is the dislocation time history. Also

$$A_4(\theta, \lambda, \delta) = \cos 2\theta \cos \lambda \sin \delta - \tfrac{1}{2} \sin 2\theta \sin \lambda \sin 2\delta \tag{2}$$

and

$$A_5(\theta, \lambda, \delta) = -\sin \theta \cos \lambda \cos \delta - \cos \theta \sin \lambda \cos 2\delta \tag{3}$$

where θ is the angle between receiver azimuth and fault strike, λ is the rake angle, and δ is the dip angle. J_1 and J_2 are the far-field step function responses for a vertical strike-slip source and a vertical dip-slip source, respectively. Expressions for J_1 and J_2 are given by Helmberger and Malone (1975). Because the far-field delta function response, $\dot{J}_j(t)$, is dominated by high-frequency reflections, we choose to display the far-field step function response, $J_j(t)$ in our figures.

When one or more layers are present, an infinite number of generalized rays are

necessary to give an exact representation of the solution at all times. The number of rays which are necessary to give a close approximation is a function of both source-to-receiver geometry and the length of record to be modeled. In order to model the first 25 sec of ground motion for three layers over a half-space and a range of 33 km, we found it necessary to include over 100 generalized rays. This number grows rapidly for an increased number of layers. Shown in Figure 6 is the strike-slip far-field step function response, $J_1(t)$, given as a function of the number of rays used in the synthetic. The number of non-degenerate rays necessary to describe responses which include rays having up to 1, 2, 3, 4, and 5 internal reflections are 4, 13, 31, 65, and 104, respectively. Here, an internal reflection is any reflection which does not occur

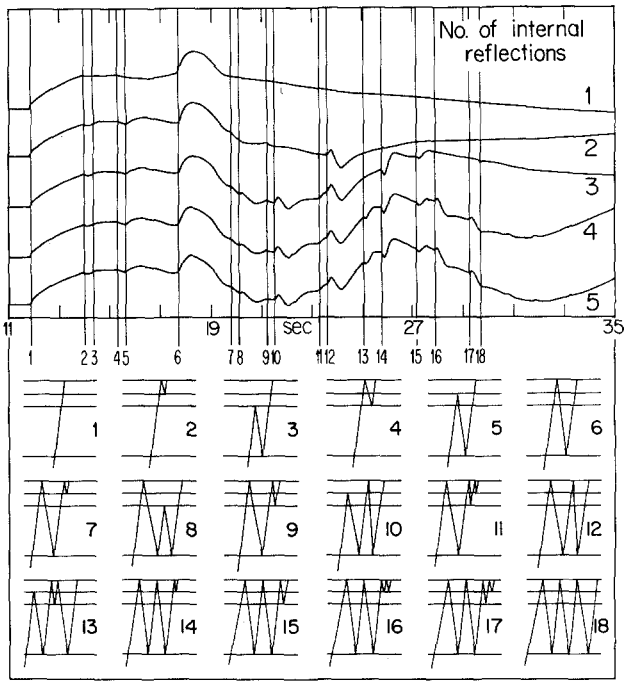

FIG. 6. Strike-slip far-field step function response as a function of the number of rays used. The number of nondegenerate rays necessary to describe responses which have up to 1, 2, 3, 4, and 5 internal reflections are 4, 13, 31, 65, and 104, respectively. An internal reflection is any reflection which does not occur at the free surface. First arrival times and schematic description of the most prominent rays are also shown. Source depth is 6.9 km and the range is 33 km.

at the free surface. It can be seen that as extra rays are added, the beginning of the response changes very little, but the latter portion of the response changes as more complex rays are added. The final summation of rays seems adequate to approximate the first 25 sec of record. Not all of these rays are of equal importance. Also shown in Figure 6 are the first-arrival times and a schematic description of the 18 most prominent phases.

Throughout this study we will stress the importance of diffraction in these models. According to Sommerfeld (1949), "Any deviation of light rays from rectilinear paths which cannot be interpreted as reflection or refraction is called diffraction." Thus head waves and the excitation of Love waves by a source exterior to the wave guide are examples of diffraction phenomena. The diffraction of spherical wave fronts can be seen in Figure 6. If geometric ray theory had been used to calculate these responses,

then they would consist of a series of steps. However, our computed responses do not consist of such sharp steps because of the inherent frequency dependence of wave propagation due to diffraction. This can be seen in the direct wave (arrival 1) which is depleted in short periods relative to long periods. This observation is important in the understanding of the spectra which we present later in this paper.

In this study, we know very little about the time history of dislocations which occurred on the fault plane of this earthquake. Because of this, we choose to consider models consisting of a single point dislocation which have time functions which give a reasonable comparison between synthetic and observed ground motion. Clearly, an earthquake is not a point dislocation. However, the differences in ground motion be-

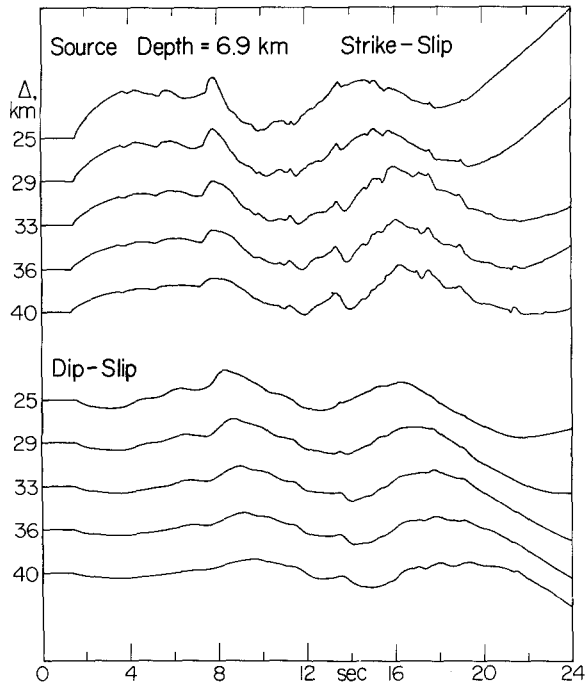

FIG. 7. Far-field step function response as a function of range. Amplitudes are scaled in relation to the top trace.

tween finite source models and point source models are for practical purposes unresolvable for this type of source-to-receiver geometry. This has been discussed by Heaton and Helmberger (1977). The reasons for this poor resolution can be understood by examining the step function responses, J_1 and J_2, as a function of source depth and epicentral range. Figure 7 demonstrates that at a constant source depth of 6.9 km, the response is a slowly varying function of range. Figure 8 shows that although the response changes more rapidly as a function of source depth, it is still a slowly changing function for depth variations of several kilometers. This generalization is particularly valid for sources occurring below the sediment layers. For sources in the sediment layers, there is a complex interference of multiply reflected rays which propagate upward and downward from the source. Thus, short-period arrivals change fairly rapidly with depth when the source occurs in the sediment layers.

A curious effect can be seen in the dip-slip responses, $J_2(t)$, displayed in Figure 8. Notice that the first motion for every response except number 5 is negative. Now

there is a radiation node for *SH* waves traveling horizontally from a vertical dip-slip fault. Rays which travel upward should be positive and rays which travel downward should be negative. The first arrivals from sources in the sediment, numbers 1 and 2, are head waves and should be negative. The first arrivals from sources in the half-space, numbers 3, 4, and 5, are direct waves and should be positive. Yet, first arrivals for sources 3 and 4 appear to be negative, and the wave form for source 5 quickly becomes negative. Somehow, energy which has traveled downward into the half-space affects the direct wave observed above the half-space. What is happening is that downgoing energy is diffracted into the sediment layers much as downgoing waves are diffracted back upward in the head wave problem. If we examine the

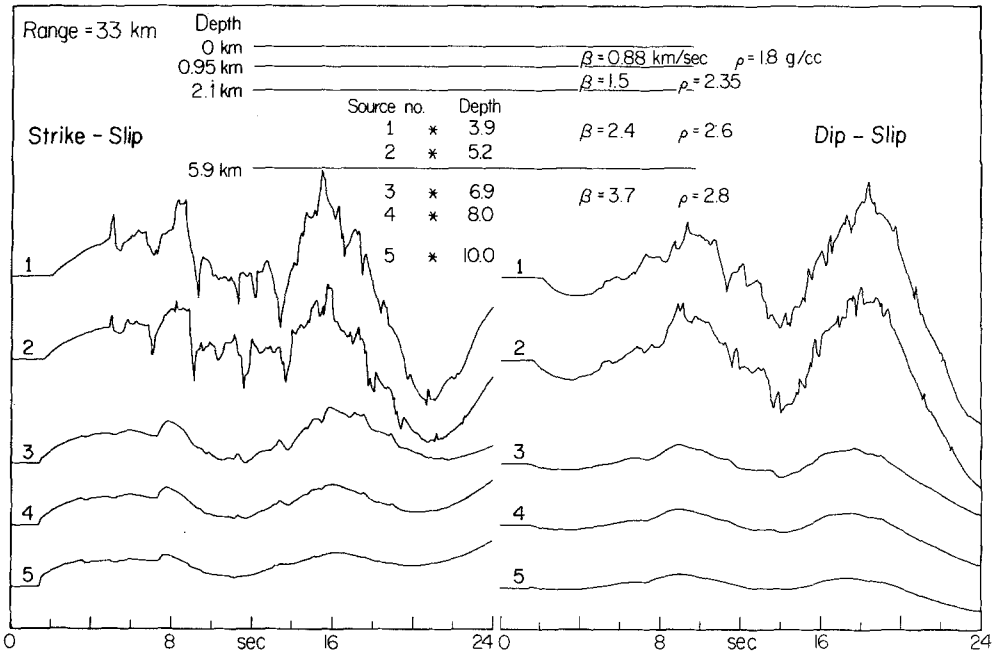

FIG. 8. Far-field step function response as a function of source depth. Amplitudes are scaled in relation to the top trace. Notice that the long-period nature of the signal changes slowly with depth, whereas short-period arrivals for sources in the sediments change rapidly.

first arrivals for source 3 in more detail, we find that it does actually break upward, but the size and duration of this first arrival is exceedingly small. The direct wave is dominated by downgoing energy which diffracted upward. Thus, where geometric ray theory would have predicted a small positive first arrival, we would actually see a fairly clear negative arrival. This example dramatically demonstrates the shortcomings of geometric ray theory for this type of problem.

Although the short-period arrivals can change rapidly with depth as mentioned earlier, the long-period character of the response is fairly stable with depth, even when the source occurs in the sediment layers. Thus, except for a travel-time correction, the response does not vary greatly along the fault plane if the dimensions of the fault are small. This observation allows us to make a formal statement which justifies modeling this earthquake with a single point source. That is, consider a fault plane with dimensions $0 < x < l$, $0 < y < h$, where x runs along the fault strike and y is down the fault dip. The tangential displacement at a receiver, $V(t)$, due to a planar

fault of arbitrary time history can be written as

$$V(t) \simeq \frac{\beta_0^2}{4\pi} \sum_{j=1}^{2} A_{j+3} \int_0^l \int_0^h \dot{S}[x, y, t - \tau(x, y)] * \dot{J}_j(x, y, t)\, dy\, dx, \tag{4}$$

where $\dot{J}_j(x, y, t)$ is the far-field delta function response of the medium, β_0 is the shear velocity in the source region, $\dot{S}[x, y, t - \tau(x, y)]$ is the time derivative (far-field response) of the dislocation history on the fault, and $\tau(x, y)$ is the time lag between the origin time of the earthquake and the initiation of rupture at the point (x, y). Equation (4) is valid as long as the source-to-receiver distance is much larger than the fault dimensions, thus ensuring that the azimuth angle from each point on the fault to the receiver is approximately constant.

Now from our previous discussion of the behavior of the point source response, $\dot{J}_j$, for small variations in x and y, we make the following approximation

$$\dot{J}_j(x, y, t) \approx \dot{J}_j[x_0, y_0, t - T(x, y)], \tag{5}$$

where

$$0 < x_0 < l, \qquad 0 < y_0 < h.$$

$T(x, y)$ is the difference in travel times between $\dot{J}_j(x, y, t)$ and $\dot{J}_j(x_0, y_0, t)$. It can easily be shown that

$$\dot{S}[x, y, t - \tau(x, y)] * \dot{J}_j[x_0, y_0, t - T(x, y)] = \dot{J}_j(x_0, y_0, t) * \dot{S}[x, y, t - \tau(x, y) - T(x, y)]. \tag{6}$$

Thus, from expressions (4), (5), and (6), we conclude that

$$V(t) \approx \frac{M_0}{4\pi\rho} \sum_{j=1}^{2} A_{j+3} [F(t) * \dot{J}_j(x_0, y_0, t)]$$

where

$$F(t) \equiv \frac{1}{lh\bar{D}} \int_0^l \int_0^h \dot{S}[x, y, t - \tau(x, y) - T(x, y)]\, dy\, dx.$$

$\bar{D}$ is the average dislocation on the fault surface. Since $V(t)$ and $J_j(x_0, y_0, t)$ are known, we can obtain some estimate for $F(t)$ through our modeling studies. Unfortunately, there is no way to deduce l, h, or $S(x, y, t)$ from a knowledge of $F(t)$. Even though a knowledge of $F(t)$ does put constraints on these parameters, any models which specify l, h, and $S(x, y, t)$ require ad hoc parameterizations of these variables.

Modeling the November 4 Brawley earthquake. We will model the November 4 earthquake with a point source located in the velocity model given in Table 1. Because of the focal mechanism given in Figure 2 and because ground motion at IVC was almost entirely tangentially polarized, we will assume that the earthquake was a pure strike-slip event occurring on a vertical plane directed toward the station, IVC. We also know that the stations IVC and ELC lie at distances of 33 and 36 km, respectively, from the epicenter. We do not have good independent constraints on either the hy-

pocentral depth or the far-field time function, $F(t)$. We will first constrain the depth to be 6.9 km and then try to estimate $F(t)$. Even though depth- and source-time function do not produce strictly independent effects in our synthetics, it is sufficient for our purposes to first estimate $F(t)$ and then to try and resolve the depth. Shown in Figure 9 are comparisons of the observed IVC tangential ground motion and synthetics with a variety of source-time functions. For simplicity, we assumed that the time function was an isosceles triangle where duration was the independent parameter. Considering the simplistic nature of the assumptions we have made about

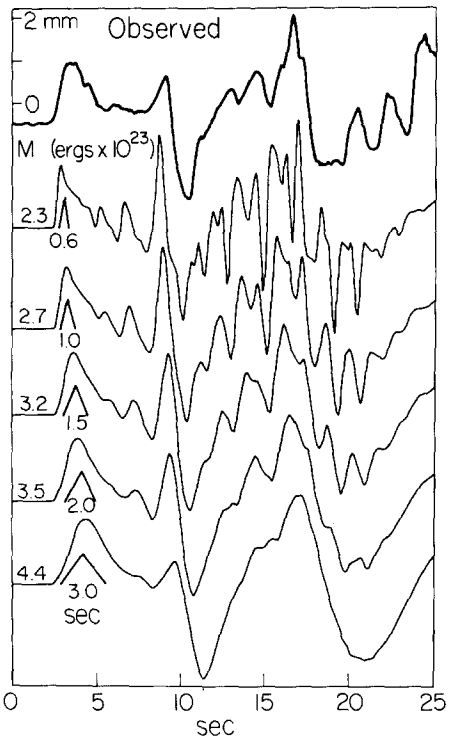

FIG. 9. Comparison of IVC tangential ground motion with synthetics which have different duration triangular far-field time functions. The far-field time functions are displayed directly under the first pulse in the corresponding synthetic. A strike-slip point source with a depth of 6.9 km and a range of 33 km was used in all of these synthetics.

velocity structure and source finiteness, it seems counter-productive to attempt more detailed modeling of the source-time function. In Figure 9, it can be seen that a duration of 1.5 sec gives the best overall fit to the observed record. Durations of 0.6 and 3.0 sec are definitely too short and too long, respectively. A moment of 3.2×10^{23} ergs is inferred if the time function is a 1.5-sec triangle. These quantities are consistent with the observations of Helmberger and Johnson (1977) concerning the empirical relationship between moment- and time-function duration.

In Figure 10 we show several comparisons of the tangential ground motions at IVC and ELC with our synthesized records. Since the beginning of the motion at ELC was not recorded, we have dotted in our guess of its shape. A far-field time function consisting of an equilateral triangle with a duration of 1.5 sec was used in the three models shown. The source depth is 6.9 km in synthetic (a) and 3.9 km in synthetic (b).

Model (a) seems to provide a good fit to both the timing and amplitudes of the major arrivals seen on the actual records. In model (a) we assumed that the source was pure strike-slip on a vertical plane directed toward IVC. Because the U.S. Geological Survey's computed hypocentral depth indicated that the source may have been somewhat shallower, in model (b) we have shown the same source that was used in model (a), but with a depth of 3.9 km. Clearly, model (b) does not fit the observed as well as model (a). The first arrival, a head wave, is too small in amplitude. Furthermore, later arrivals come in too soon with respect to the first arrival. It is possible to improve the shallow source depth synthetic wave forms by changing the fault orientation. A fault plane striking at N39°W, dipping 60° to the SW, with a rake angle of 120°, and a depth of 3.9 km was assumed in model (c). This improves the fit, but the timing of arrivals is still inferior when compared to model (a). Furthermore, model

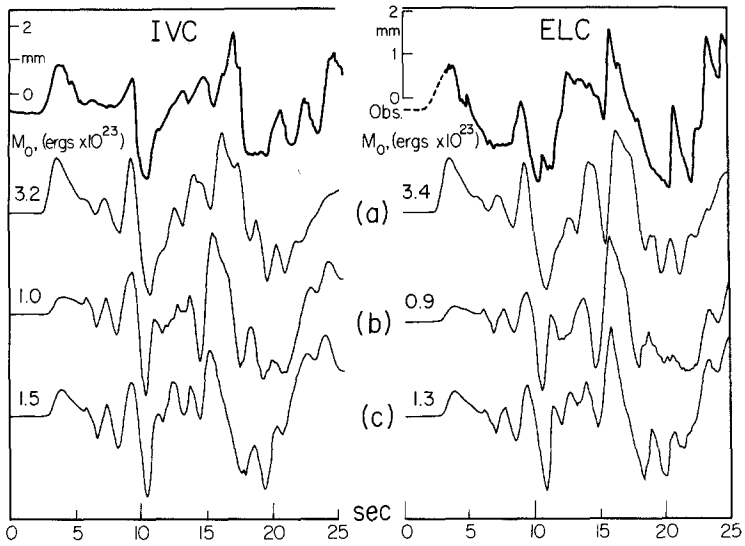

FIG. 10. Comparisons of IVC and ELC tangential ground motions with synthetics. IVC and ELC are assumed to be at ranges of 33 and 36 km, respectively. A triangular far-field time function with a duration of 1.5 sec is used throughout. (a) Pure strike-slip with source depth of 6.9 km. (b) Pure strike-slip with source depth of 3.9 km. (c) Source depth of 3.9 km and source striking N39°W, dipping 60°SW, and with a rake of 120°.

(a) is consistent with the change in amplitude ratios of tangential-to-radial ground motion seen between IVC and ELC. Model (c) is consistent with neither of these ratios nor with the focal mechanism given in Figure (2). For this reason, we prefer model (a) with a focal depth of 6.9 km.

At this point, let's step away from all of these modeling details and try to evaluate where we've been. We have approximated the shear-wave velocities in a 6-km thick stack of sediments with three planar layers over a half-space. Our simplified shear-wave model is based on compressional wave refraction studies. We argued that, in this case, a $M4.9$ earthquake could be approximated by a point source with the appropriate time function. The distances between source and receiver are well constrained by the U.S. Geological Survey's epicentral solution. Our focal mechanism constrains our dislocation model to be predominantly strike-slip on a vertical plane. The source-time function and depth are variables which we were able to constrain only through our modeling studies. Although a fairly large suite of models could be constructed by varying the depth and time function, it seems clear that the match

between model (a) and the observed ground motion was not a mere coincidence. Apparently, the assumptions which lead to model (a) were sufficiently valid to predict the tangential ground motions seen at ELC and IVC. We could even argue that, given the moment, the time function would have been predicted accurately by the moment versus duration plot given by Helmberger and Johnson (1977). Considering this success, we feel that it should be possible to make predictions of the tangential ground motions seen in the Imperial Valley. Because one must *a priori* know such variables as hypocentral location, fault mechanism, and source-time function, there is some question about the practical applications of such predictions. Our simplistic modeling of source and structure necessarily limits such predictions to longer period motions. In order to model large earthquakes, source finiteness would also have to be considered. As we have already seen, the ability to predict the effects of structure provides valuable insight into the problem of determining source depth and time function.

Now that you're thoroughly tired of hearing our inflated claims of success, we'll discuss our failures. We say that we've constructed a model to explain the first 25 sec of observed motion. What about motions occurring 60 sec into the record? Here we fail, for our model would predict practically no motion after 35 sec. Long duration codas are routinely observed on nearly all local earthquake records. Their causes are not well understood. Long-period P-wave forms recorded at several Canadian stations show a relatively simple pulse for the P wave of this earthquake. Thus, there seems to be no justification for producing this coda by assuming that this earthquake was a complicated multiple event. Perhaps the coda is due to surface waves which are reflected by lateral variations in structure. In Figure 3, it can be seen that at IVC, even the coda is tangentially polarized with respect to the epicentral location. This observation is hard to understand if the coda is due to waves which are reflected off the boundaries of the Salton trough since we would presumably see a Rayleigh wave contribution along with the Love waves.

Synthetic Fourier spectra. We will now discuss the effects of plane layered velocity structure upon the Fourier amplitude spectra of ground displacement. In a homogeneous half-space, the far-field *SH* response to a point step dislocation is simply a delta function whose Fourier amplitude spectrum is some constant value at all frequencies. If the earth were this simple, then the amplitude spectra of *SH* ground motion would accurately reflect the amplitude spectra of only the source. As we have already seen, the introduction of layering produces profound changes in the far-field delta function response. It has been commonly assumed that the effects of structure do not change the overall shape of amplitude spectra (for examples, see Johnson and McEvilly, 1974, or Tucker and Brune, 1973). The justification given is that all of the arrivals on a seismogram are caused by the same source and thus each arrival contains the spectral characteristics of the source. Interference between various arrivals should introduce irregularities into the spectra (spectral scalloping), but this interference phenomena should not change the overall shape of the spectra. In order to test the validity of this assumption, we have computed the Fourier amplitude spectra of the *SH* far-field delta function responses of point sources located in the layered half-space which is described in Table 1. If the above assumption is correct, then the synthetic spectra should be basically flat. In Figure 11, we show synthetic spectra for a point source located at a range of 33 km and at depths of 3.9, 6.9, and 10 km. Here we have plotted the function, $\|F \cdot T \cdot (\dot{J}_j)\|$, where $\dot{J}_j(t)$ is the far-field delta function response used in equation (1). Spectra of both strike-slip and dip-slip terms are shown.

The corresponding spectra for a homogeneous half-space are given by the straight dotted lines. When the source is in the sedimentary layers, the spectra appear to be relatively flat with complicated scalloping. In the strike-slip case, the layered space produces a long-period level which is 2 or 3 times the level computed for a homogeneous half-space. The sedimentary layers have trapped energy of all frequencies. In the dip-slip case, the layered space produces a long-period level which is an order of

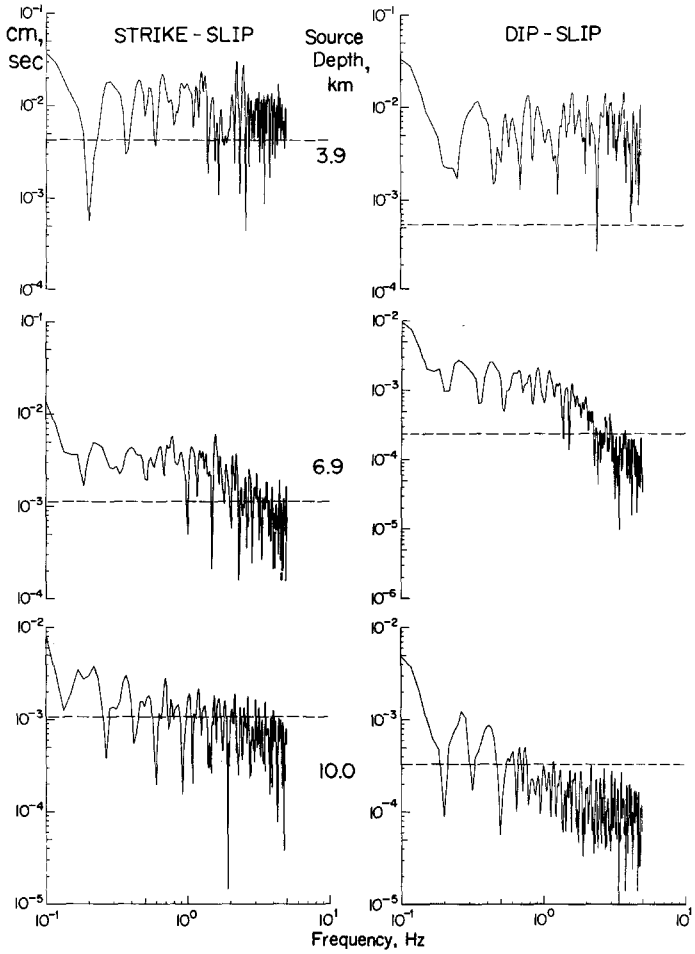

FIG. 11. Synthetic far-field delta function responses as a function of source depth, where the range is 33 km. Dotted lines indicate corresponding half-space responses.

magnitude higher than is produced by the homogeneous half-space. This discrepancy is primarily caused by the fact that, in the homogeneous case, the direct *SH* ray is very near a radiation node. Waves which are reflected within the sediments traverse paths which are much farther from this node. When the source is moved to a depth of 6.9 km (1 km beneath the sediments), the spectra no longer look flat. In fact, it appears that we could pick corner frequencies in these spectra. This is remarkable when one realizes that these are delta function responses! There appears to be an ω^{-1} and ω^{-2} falloff in the high frequencies for the strike-slip and dip-slip cases, respectively. The reason for this behavior is hard to understand from the viewpoint of geometric ray theory. What we see here is actually a diffraction effect. Long-period

energy is diffracted into and trapped within the sediment layers, while shorter period energy is reflected off the bottom of the sediments. When the source is moved to a depth of 10 km, we see another dramatic change in the shape of the spectra. Diffraction effects are responsible for the slope seen for longer periods. For this depth, geometric ray theory is probably adequate to explain very short-period wave forms. This is consistent with the fact that the spectra become relatively flat for short periods. Our interpretations are further complicated by the effects of radiation pattern.

We have seen that, at a constant epicentral range, the effects of depth are dramatic. In Figure 12, we show spectra for sources at a constant depth of 6.9 km and at ranges of 25 to 40 km. Apparently range also has a large effect upon the overall spectral shape. Clearly this has implications for seismic wave attenuation studies as well as

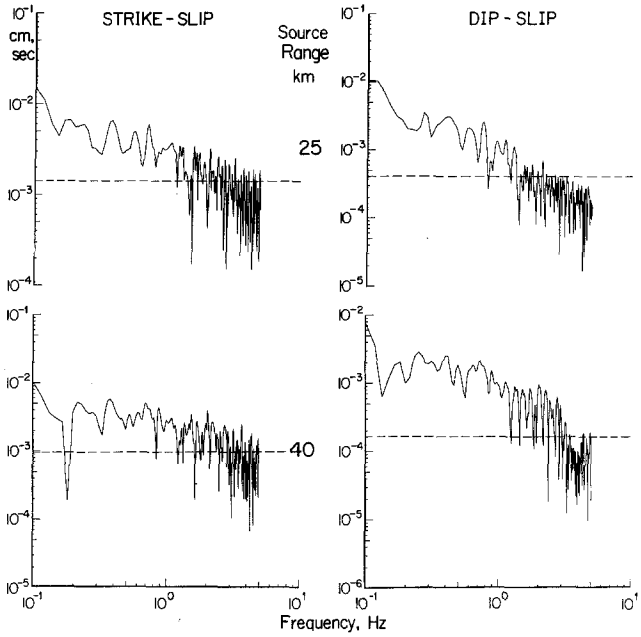

FIG. 12. Synthetic far-field delta function responses as a function of range. Source depth is 6.9 km. Dotted lines indicate corresponding half-space responses.

seismic source studies. Remember, there is no anelasticity built into our synthetic models.

In the case of *SH* waves, we have seen that the introduction of layering can do far more than simply add scalloping to a spectrum. The exact effect is a complicated function of the source location and focal mechanism. Although we have only demonstrated this to be true for whole-record spectra, the spectra of individual arrivals should also be affected by diffraction phenomena. Even if the direct *S* wave could be isolated, there is no guarantee that the wave form has not been altered by diffraction effects. This can be seen by noticing that the step function response of the direct *S* wave does not consist of a simple step. Furthermore, if one desires to understand the high-frequency characteristics of the source, then one must understand the high-frequency effects of wave propagation. This means that one must know the details of the velocity structure along with a good estimate of source location. Because the effects of wave propagation are so complicated, we prefer to do our modeling in the time domain. Although ambiguities are still present when trying to sort out the rela-

tive effects of source and structure, there is some hope of understanding the effects of wave propagation when modeling in the time domain. We anticipate that the phenomena which we have observed for *SH* waves should also be seen for *P* and *SV* waves. Because of the existence of mode conversions and Rayleigh waves, the effects of wave propagation will be even more complicated for radial and vertical motions.

Conclusions

The sedimentary structure which lies between the $M4.9$ November 4, 1976 earthquake and the stations, IVC and ELC, is relatively flat. A simplified model of shear-wave velocities was derived from the compressional wave refraction studies of Biehler *et al.* (1964). The epicentral solution and focal mechanism were determined by *P*-wave first-arrival studies. Using these constraints, we determined a hypocentral depth of about 7 km by modeling the tangentially polarized ground motions observed at IVC and ELC. An infinitesimal dislocation source with a triangular time function was sufficient to model the first 25 sec of observed ground motion. We determined the moment to be approximately 3×10^{23} ergs and the far-field time function had a duration of about 1.5 sec. Because of our success in modeling these records, we feel that propagational effects on longer period tangential ground motions are predictable in the Imperial Valley. We also found that our layered half-space model was unable to explain the long-duration codas seen at IVC and ELC.

By studying the Fourier amplitude spectra of the far-field delta function responses computed for our layered half-space model, we demonstrated that wave propagation effects should be included in studies of source spectra. Diffraction phenomena can produce corners which have nothing to do with source spectral characteristics. The effects of structure must also be included when making estimates of the moment from the long-period level of amplitude spectra. Finally, the effects of diffraction should be considered in studies of seismic wave attenuation.

Acknowledgments

We wish to thank H. Kanamori for bringing the IVC record to our attention and for critically reading the manuscript. We would also like to thank G. Brady of the U.S. Geological Survey for providing copies of the ELC record and also H. Wasson of Imperial Valley College for his assistance with the station IVC. M. Schnapp and G. Fuis provided useful discussion and information regarding the hypocentral location of the earthquake. We are particularly grateful to S. Biehler for supplying important information and figures concerning the velocity structure in the Imperial Valley.

This research was supported by the National Science Foundation EVN76-10506. Operating funds for the torsion seismometer at IVC are provided by U.S.G.S. Survey Contract 14-08-001-15893.

References

Biehler, S. (1964). Geophysical study of the Salton Trough of Southern California, *Ph.D. Thesis*, California Institute of Technology, Pasadena.

Biehler, S., R. L. Kovach, and C. R. Allen (1964). Geophysical framework of the northern end of the Gulf of California structural province, in *Marine Geology of Gulf of California*, T. Van Andel and G. Shor, Editors, *Am. Assoc. Petrol. Geologists Mem.* **3**, 126–196.

Heaton, T. H. and D. V. Helmberger (1977). A study of the strong ground motion of the Borrego Mountain, California, Earthquake, *Bull. Seism. Soc. Am.* **67**, 315–330.

Helmberger, D. V. (1974). Generalized ray theory for shear dislocations, *Bull. Seism. Soc. Am.* **64**, 45–64.

Helmberger, D. V. and S. D. Malone (1975). Modeling local earthquakes as shear dislocations in a layered half-space, *J. Geophys. Res.* **80**, 4881–4888.

Helmberger, D. V. and L. R. Johnson (1977). Source parameters of moderate size earthquakes and the importance of receiver crustal structure in interpreting observations of local earthquakes, *Bull. Seism. Soc. Am.* **64**, 301–313.

Hudson, D. E., A. G. Brady, M. D. Trifunac, and A. Vijayaraghavan (1971). Strong-motion earthquake accelerograms, corrected accelerograms and integrated velocity and displacement curves, Vol. II, Part A, Earthquake Eng. Res. Lab., *EERL 86–88*, California Institute of Technology, Passadena, California.

Johnson, C. E. and D. M. Hadley (1976). Tectonic implications of the Brawley Earthquake Swarm, Imperial Valley, California, January 1975, *Bull. Seism. Soc. Am.* **66**, 1133–1144.

Johnson, L. R. and T. V. McEvilly (1974). Near-field observations and source parameters of Central California earthquakes, *Bull. Seism. Soc. Am.* **64**, 1855–1886.

Sharp, R. V. (1976). Surface faulting in Imperial Valley during the earthquake swarm of January-February, 1975, *Bull. Seism. Soc. Am.* **66**, 1145–1154.

Sommerfeld (1949). *Optics*, Academic Press, Inc., New York, 383 pp.

Tucker, B. E. and J. N. Brune (1973). *S*-wave spectra and source parameters for aftershocks of the San Fernando earthquake of February 9, 1971, in *Geological Geophysical Studies*, Vol. 3, *San Fernando Earthquake of February 9, 1971*, NOAA, U. S. Dept. of Commerce, Washington, D. C.

Vered, M. and A. Ben-Menahem (1974). Application of synthetic seismograms to the study of the low-magnitude earthquakes and crustal structure in the northern Red Sea Region, *Bull. Seism. Soc. Am.* **64**, 1221–1237.

Division of Geological and Planetary Sciences
California Institute of Technology
Pasadena, California 91125
Contribution No. 2929

Manuscript received July 19, 1977